Observations of Galactic and Extra-galactic Sources From the BOOMERANG and SEST Telescopes

K. Coble[1,2], P.A.R. Ade[3], J.J. Bock[4], J.R. Bond[5], J. Borrill[6], A. Boscaleri[7], C. R. Contaldi[5], B.P. Crill[8], P. de Bernardis[9], P. Farese[10], K. Ganga[11], M. Giacometti[9], E. Hivon[11], V.V. Hristov[11], A.H. Jaffe[12], W. C. Jones[11], A.E. Lange[11], L. Martinis[13], S. Masi[9], P. Mason[11], P.D. Mauskopf[14], A. Melchiorri[9], T. Montroy[15], C.B. Netterfield[16], L. Nyman[17,18] E. Pascale[7], F. Piacentini[9], D. Pogosyan[5], G. Polenta[9], F. Pongetti[9], S. Prunet[5], G. Romeo[19], J.E. Ruhl[20], F. Scaramuzzi[13]

ABSTRACT

[1]Dept. of Astronomy and Astrophysics, University of Chicago, 5640 South Ellis Ave., Chicago, IL 60615, USA, coble@hyde.uchicago.edu

[2]Adler Planetarium and Astronomy Museum, 1300 South Lake Shore Drive, Chicago, IL 60605, USA

[3]Queen Mary and Westfield College, London, UK

[4]Jet Propulsion Laboratory, Pasadena, CA, USA

[5]Canadian Institute for Theoretical Astrophysics, University of Toronto, Canada

[6]National Energy Research Scientific Computing Center, LBNL, Berkeley, CA, USA

[7]IROE-CNR, Firenze, Italy

[8]Physics Dept., California State University, Dominguez Hills, Carson, CA, USA

[9]Dipartimento di Fisica, Universita' La Sapienza, Roma, Italy

[10]Princeton University, Princeton, NJ, USA

[11]California Institute of Technology, Pasadena, CA, USA

[12]Center for Particle Astrophysics, University of California, Berkeley,CA, USA

[13]ENEA Centro Ricerche di Frascati, Via E. Fermi 45, 00044, Frascati, Italy

[14]Dept. of Physics and Astronomy, Cardiff University, Cardiff, Wales, UK

[15]Dept. of Physics, University of California, Santa Barbara, CA, USA

[16]Depts. of Physics and Astronomy, University of Toronto, Canada

[17]Swedish-ESO Submillimetre Telescope (SEST), European Southern Observatory, Casilla 19001, Santiago, CHILE

[18]Onsala Space Observatory, SE-439 92 Onsala, Sweden

[19]Istituto Nazionale di Geofisica, Roma, Italy

[20]Physics Dept., Case Western Reserve University, Cleveland, OH, USA

We present millimeter-wave observations of three extra-galactic and six Galactic sources in the Southern sky. Observations were made at 90, 150, 240 and 400 GHz with resolutions of 18, 10, 14 and 12 arcmin respectively during the 1998 Antarctic long duration balloon flight of BOOMERANG. Observations were also made with the SEST telescope, at 90 and 150 GHz with resolutions of 57 and 35 arcsec respectively. These observations can be used for calibrations of Cosmic Microwave Background (CMB) experiments as well as an understanding of the physical processes of the sources.

Subject headings: ISM: HII regions – Extra-galactic: point sources – general: microwave observations

1. Introduction

Galactic millimeter-wave radiation arises from a combination of synchrotron, free-free and dust emission. Compact millimeter-wave sources in the Galaxy can potentially be used to calibrate observations of the Cosmic Microwave Background (CMB). Southern Galactic sources are particularly useful for CMB observations that take place in the Antarctic, where planets are observed only at low elevation. Previous millimeter-wave observations of Southern Galactic sources have been made by Arnold et al. (1978), Cheung et al. (1980), Cox et al. (1995), Ruhl et al. (1995), and Puchalla et al. (2002). For reviews of radio observations of a subset of our Galactic sources, see e.g. Brooks et al. (1998) and De Pree et al. (1999). Extra-galactic point sources are expected to be an important foreground contaminant of CMB observations (Toffolatti et al 1999, Sokasian et al. 2001).

BOOMERANG is a millimeter-wave telescope and receiver designed to measure anisotropy in the Cosmic Microwave Background (CMB) from the Long Duration Balloon (LDB) platform. BOOMERANG launched from McMurdo station, Antarctica on December 29, 1998 for a 10.5 day flight. The instrument is described in detail in Crill et al. (2002). CMB angular power spectrum results can be found in de Bernardis et al. (2000), Netterfield et al. (2002) and Ruhl et al. (2002). Diffuse dust is discussed in Masi et al. (2001). In addition to observing the CMB, BOOMERANG observed three extra-galactic point sources and six Galactic compact HII regions. The flux measurement of these sources are calibrated with the CMB dipole. Follow-up observations of the three extra-galactic sources and two of the Galactic sources were made using the SEST telescope at La Silla Observatory in Chile, January 8-10, 2000. A list of sources and coordinates are given in Table 1.

2. BOOMERANG Observations and Results

The BOOMERANG telescope features a 1.2m primary mirror and a cryogenic bolometric array receiver. There are two 90 GHz detectors, both with a FWHM of 18±1 arcmin, six 150 GHz detectors, with FWHMs of 9.2±0.5, 9.2±0.5, 9.7±0.5, 9.4±0.5, 9.9±0.5, and 9.5±0.5 arcmin, three 240 GHz detectors with a FWHM of 14.1±1 arcmin, and four 400 GHz detectors with a FWHM of 12.1±1 arcmin. The main lobes of the beams from the 90, 150, and 400 GHz channels are well-characterized by single Gaussians. The 240 GHz beams have a supressed central region, accurately modeled by the superposition of one Gaussian to fit the full beam plus an inverted Gaussian that improves the fit in the central region. Long term random pointing drift does not add significantly to the beam size for the Galactic sources, since each of those observations were made on a short timescale. The extra-galactic sources however, are affected by long-term random pointing drifts, because those observations were made throughout the flight. A pointing uncertainty of 2.5 arcmin rms adds in quadrature to the effective beam size and adds 1.4 arcmin rms to the beam uncertainty for the extra-galactic sources. See Netterfield et al. (2002) for a more detailed discussion of pointing uncertainty. The 90, 150, and 240 GHz channels are calibrated using the CMB dipole, with an uncertainty of 10% to diffuse beam-filling sources. The 400 GHz channels are calibrated using interstellar dust and degree-scale CMB anisotropy, with an uncertainty of 30% (Crill et al. 2002).

Observations with BOOMERANG are made by scanning the telescope at an angular velocity of 2 degrees/sec in azimuth for the first half of the flight and 1 degree/sec in azimuth for the second half of the flight. Interspersed between CMB observations are observations of the Galactic plane. The Galactic sources were observed at the same scan speeds as the CMB observations, but with shorter scans (10 degrees peak-to-peak in azimuth for the source scans vs. 60 degrees peak-to-peak for the CMB scans). In total there were 15 Galactic source scans: one of the Carina Nebula, four of RCW38, four of IRAS1022, five of IRAS08576 and one which included both NGC3603 and NGC3576. Nearly (but not quite) all of the data for all of the detectors was good for each scan; Table 1 lists the number of good observations (which includes the number of good scans and channels) at each frequency. Scans of the Galactic sources were flagged as bad for a particular channel for example if the source was on the edge of the scan in that channel. The extra-galactic sources were observed serendipitously during the CMB scans during the entire flight. The total number of good observations of the extra-galactic sources in Table 1 reflects the number of channels at each frequency in which the source was detected.

BOOMERANG maps of the Galactic sources are shown in Figure 1. Each of the maps shown are 3 degrees × 3 degrees in extent and represent only one channel of data for one

scan (approximately 15 minutes of data). Other scans are similar and the total number of observations for each source at each frequency are given in Table 1 The maps are flat space projections centered on the source, with coordinates given by ($x = (\alpha - \alpha_0)cos(\delta)$, $y = (\delta - \delta_0)$), where (α_0, δ_0) are the Right Ascension and declination of the sources given in Table 1. IRAS 100 μm maps (data obtained through the Skyview website) of the same regions are included for comparison. From the Galactic source maps, NGC3576 is the most compact of our sources, followed by RCW38. IRAS1022 and especially the Carina Nebula show significant extended emission. IRAS08576 shows significant extended emission along a line; this is unexpected from IRAS 100 μm data, which shows IRAS08576 as a compact object. In the maps there are bright, compact sources typically surrounded by more diffuse clouds. Fluxes are measured for the bright, compact sources in each map.

The Galactic source maps for each scan and channel are binned in radius around the centroid of the source to obtain the integrated flux as a function of radius. A sample radial flux profile for one source and frequency is shown in Figure 2. Following the notation of Puchalla et al. (2002), we calculate the total integrated flux within radii of 1 and 2 σ_{beam} (hereafter $1\sigma_b$ and $2\sigma_b$ fluxes). The beam size is given by $\sigma_{beam} = FWHM/(2\sqrt{2ln2})$ and the FWHMs of the detectors are given above. When computing fluxes for NGC3603 and NGC3576, the companion source is masked out in the map.

Table 2 lists the $1\sigma_b$ and $2\sigma_b$ fluxes for all sources and frequencies. The flux and uncertainty for the Galactic sources in Table 2 are the mean and standard deviation of all of the good channels and scans at the given frequency. Only the statistical uncertainty is given in the table. Uncertainty in the flux due to calibration is not included. The $1\sigma_b$ and $2\sigma_b$ flux results are systematically dependent on beam at approximately the 10% and 5% level, respectively. The fluxes are dependent on background subtraction at about the 1% level. The uncertainty in the flux due to the inherent S/N of the data is approximately 2%.

Since the S/N on the extra-galactic sources is much lower than the S/N on the Galactic sources, maps are not used in this analysis; fluxes are computed directly by binning the timestream data in radius, after filtering at 0.2 Hz. Since there are relatively few observations of each source (see Table 1) and since the S/N of each observation is low, *weighted* means and standard deviations are given in Table 2. Background subtraction systematically affects the $1\sigma_b$ and $2\sigma_b$ fluxes by about 10% and 25% respectively. Uncertainty in the beam systematically affects the $1\sigma_b$ and $2\sigma_b$ fluxes by approximately 30% and 25% respectively.

If the flux of the source scales as $f \propto \nu^\alpha$, then the spectral index, $\alpha_{1:2}$, between frequencies ν_1 and ν_2, is given by:

$$\alpha = \frac{log(f_2/f_1)}{log(\nu_2/\nu_1)}. \tag{1}$$

Spectral indices for the BOOMERANG $1\sigma_b$ and $2\sigma_b$ fluxes are given in Table 3.

3. Wavelet Analysis of the Extra-galactic Sources

In addition to the analysis in the previous section, a wavelet approach is also used, following Vielva et al. (2001), to evaluate the fluxes and the spectral indices for the three extra-galactic point sources observed by BOOMERANG. The main advantages of using this method are the amplification of the signal to noise ratio and that the result is only sensitive to sources of size equal to or smaller than the beam, so the measured fluxes are much less affected by the background signal.

The isotropic wavelet transform for a two-dimensional map $T(\mathbf{x})$ is defined by:

$$w_T(R, \mathbf{p}) = \int d^2\mathbf{x} \frac{1}{R^2} \psi \left(\frac{|\mathbf{x} - \mathbf{p}|}{R} \right) T(\mathbf{x}) \tag{2}$$

where $w_T(R, \mathbf{p})$ is the wavelet coefficient of the map T associated with a scale R and centered at the point $\mathbf{p}$. The function $\psi(|\mathbf{x}|)$ is called the wavelet mother function. If the beam profile is Gaussian it is found that Mexican Hat wavelet is the optimal one. The mother function is then

$$\psi(x) = \frac{1}{\sqrt{2\pi}} \left[2 - \left(\frac{2}{R} \right)^2 \right] e^{\frac{x^2}{2R^2}} \tag{3}$$

and has zero integral. Substituting eq. 3 into eq. 2, for a point source centered on $\mathbf{y}$ yields

$$w_T^{th}(R, \mathbf{y}) = 2\sqrt{2\pi} \frac{A}{\Omega} \frac{(R/\sigma_b)^2}{(1 + (R/\sigma_b)^2)^2} \tag{4}$$

where Ω is the area under the Gaussian beam, σ_b is the beam dispersion and A is the flux of the point source. In order to estimate the point source flux, A, a multi-scale fit is performed computing the wavelet coefficients of our map, centered in the nominal coordinates of the source, at a number of scales R. The results are compared with the theoretical curve given by eq. 4 using the χ^2 statistic:

$$\chi^2 = \left[w_T(R_i, \mathbf{y}) - w_T^{th}(R_i, \mathbf{y}) \right] C^{-1}(R_i, R_j) \left[w_T(R_j, \mathbf{y}) - w_T^{th}(R_j, \mathbf{y}) \right] \tag{5}$$

where the covariance matrix C is computed using real data:

$$C_{ij} = \langle w_T(R_i, \mathbf{x}) w_T(R_j, \mathbf{x}) \rangle \tag{6}$$

and the average is performed over random positions $\mathbf{x}$.

In order to check the effect of a non-Gaussian beam on the results, the analysis has been done on simulated point sources with different beam shapes. The error in the flux recovery is smaller than 10% even for a highly non-Gaussian beam, such as a square or triangular beam, if there is a good estimation of the integrated beam, Ω, in eq. 4.

Spectral indices are computed from the fluxes according to eq. 1. The flux and spectral index results are given in Table 4 and are in good agreement with the radial integration results of the previous section.

4.   SEST Observations and Results

Point source observations of the three extra-galactic sources and images of the Galactic sources RCW38 and NCG3576 at 90 and 150GHz were made with the SEST telescope at La Silla Observatory in Chile on January 8-10, 2000. The FWHM of the SEST 90 GHz beam is 57 arcsec, the FWHM of the SEST 150 GHz beam is 35 arcsec and the chop is 11 arcmin. Calibration was done using the chopper wheel method. The antenna temperature scale, given in T_{A*}, was converted to a flux density scale through observations of planets (SEST web page).

For the Galactic sources NGC3576 and RCW38, observations were made in a region 4'x4' in extent centered on each source with a grid spacing of 17.5 arcsec (hereafter center maps). Additional observations were made with a wider grid spacing (35 arcsec) covering a larger region around each source (10 arcmin x 10 arcmin in extent for NGC3576, 6 arcmin x 6 arcmin in extent for RCW38) (hereafter extended maps). For RCW38, the more extended of the two sources, the center and extended observations were combined. For NCG3576 only the center maps were used, since the data far from the source are noisy or could be contaminated by objects outside the field.

Maps are shown in Figure 3 and fluxes are given in Table 5. Again, maps are a flat-space projection centered on the source, as in Figure 1. Fluxes for RCW38 and NGC3576 are computed within the map regions. Fluxes for the extra-galactic sources are from point source observations. Spectral indices are computed from the fluxes using eq. 1 and are also given in Table 5.

The SEST observations can be convolved with the BOOMERANG beam in order to check the BOOMERANG calibration. For RCW38 and NGC3576, the SEST maps are convolved with the BOOMERANG beam and flux profiles are obtained from the convolved maps. A numerical convolution is not necessary for the extra-galactic sources since the analytic convolution of a point source with a Gaussian is simple; the 1 σ_b and 2 σ_b fluxes

should be 0.393 and 0.865 of the point source flux. Flux ratios are given in Table 6, where the BOOMERANG fluxes used are those from Table 2. The extra-galactic sources may be time variable, and since the BOOMERANG and SEST observations were made approximately a year apart, they could have different intensities not only because of calibration but because of intensity variations. From a weighted mean of the numbers in Table 6, the current BOOMERANG calibration relative to SEST is 0.97±0.07 for the 90 GHz channels and 1.04±0.06 for the 150 GHz channels. In other words, the BOOMERANG and SEST calibrations agree with each other to within the uncertainties.

The MAT team has published fluxes for NGC3576 at 150GHz (Puchalla et al. 2002). For MAT, $\sigma_{beam} = 12.14/(2\sqrt{2ln2}) = 5.16$ arcmin. The ratio MAT/(SEST*MAT) for the NGC3576 150 GHz observations is 1.01±0.14 and 1.00±0.15 for their $1\sigma_b$ and $2\sigma_b$ fluxes respectively, implying that SEST and MAT agree well. Therefore, the calibrations of BOOMERANG, SEST and MAT are all consistent for NGC3576 at 150 GHz.

5. Conclusions

A comparison with the SEST data for the Galactic sources NGC3576, RCW38 and extra-galactic sources 0537-441, 0521-365 and 0438-43 implies that the current BOOMERANG calibration and SEST agree to within 8% at 90 GHz and 6% at 150 GHz. Additionally, BOOMERANG, MAT, and SEST fluxes of NGC3576 at 150 GHz are all consistent with each other.

The Galactic sources typically show a flat to inverted spectrum from 90 to 150 GHz and a rising spectrum from 150 to 240 GHz and from 240 to 400 GHz. This is consistent with a combination of free-free and dust emission, with free-free dominating at the lower frequencies and dust dominating at higher frequencies. Our spectral indices are consistent with the typical $f \propto \nu^2$ expected for millimeter observations of HII regions. While the uncertainties on the spectral indices of the extra-galactic sources from BOOMERANG are large, the SEST measurements imply a falling spectrum with increasing frequency. To place these measurements in context, Figure 4 shows the extra-galactic source fluxes along with measurements from a wide range of the electromagnetic spectrum.

REFERENCES

Arnold, E. M., Kreysa, E., Schultz, G. V., Sherwood, W. A. 1978, A&A, 70, L1

Brooks, K. J., Whiteoak, J. B., & Storey, J. W. V. 1998, PASA, 15, 202

Cheung, L. H., Frogel, J. A., Gezari, D. Y., & Hauser, M. G. 1980, ApJ, 240,74

Condon, J. J., Griffith, M. R., & Wright, A. E. 1993, AJ, 106, 1095

Cox, P., Mezger, P. G., Sievers, A., Najarro, F., Bronfman, L., Kreysa, E., & Haslam, G. 1995, A&A, 297, 168

Crill, B. P., et al. 2002, submitted to ApJ, `astro-ph/0206254`

deBernardis, P. et al. 2000, Nature, 404, 955

DePree, C. G., Nysewander, M. C., & Goss, W. M. 1999, AJ, 117, 2902

Masi, S., et al. 2001, `astro-ph/0101539`

NASA/IPAC Extra-galactic Database (NED), `http://nedwww.ipac.caltech.edu`

Netterfield et al. 2002, ApJ, 571, 604

Puchalla, J. et al. 2002, AJ, 123, 1978

Ruhl, J. E., et al. 2002, `astro-ph/0212229`

SEST web page: `http://www.ls.eso.org/lasilla/Telescopes/SEST/SEST.html`

Sokasian, A., Gawiser, E. & Smoot, G. F. 2001, ApJ, 562, 88

Skyview, IPAC, `http://skyview.gsfc.nasa.gov/`

Toffolatti, L., De Zotti, G., Argueso, F., & Burigana, C. 1999, `astro-ph/9902343`, invited review in "Microwave Foregrounds", eds. A. de Oliveira-Costa and M. Tegmark (ASP, San Francisco, 1999)

Vielva, P., et al. 2001, MNRAS, 328, 1
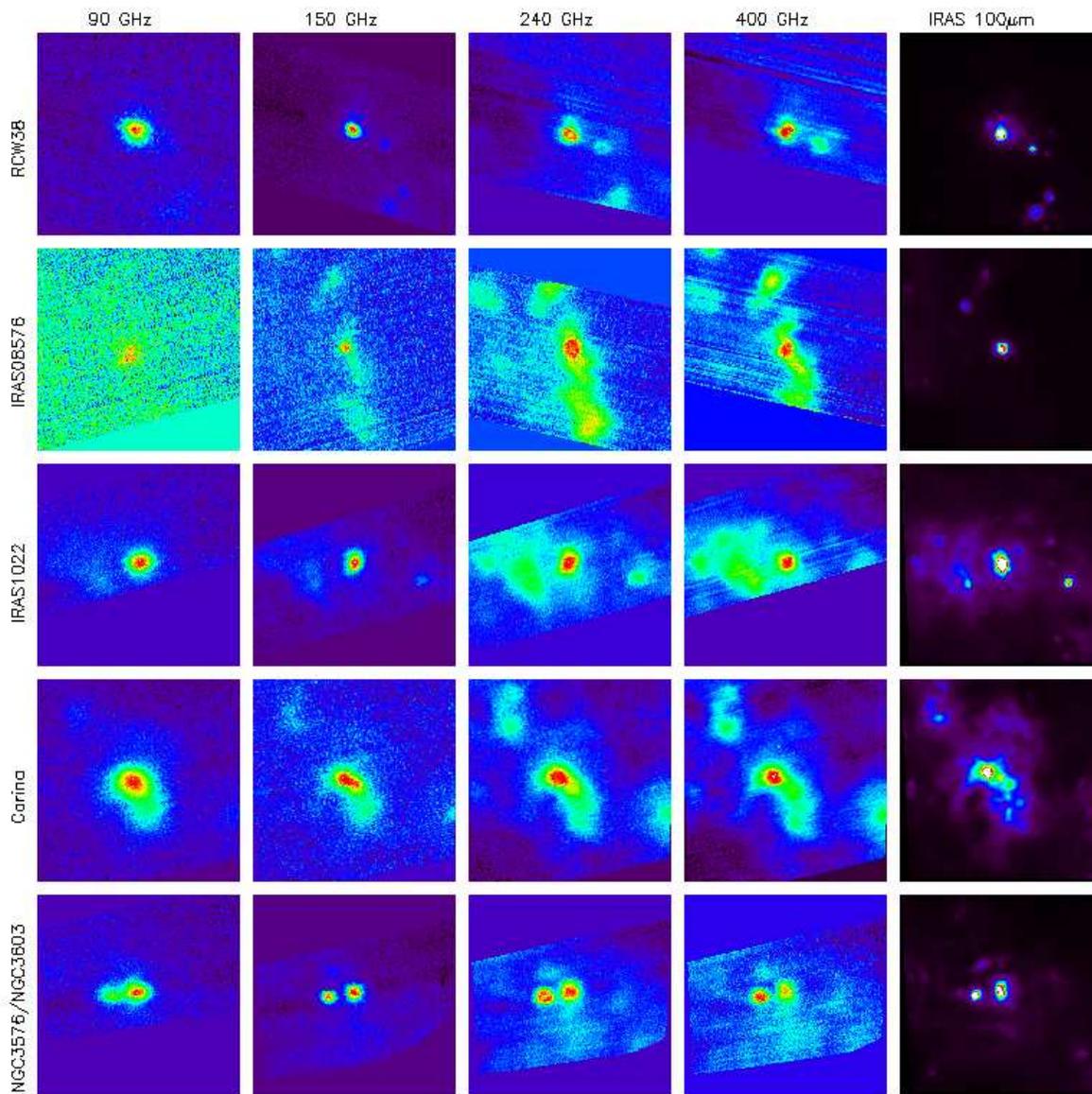
Fig. 1.— BOOMERANG maps of the Galactic sources, made from data from a single scan and a single channel. Other observations for each source and frequency are similar and the total number of observations for each source at each frequency are given in Table 1. IRAS 100 μm maps are included for comparison. The images are all $3° \times 3°$ in extent. The maps are flat space projections centered on the source, with coordinates given by $(x = (\alpha - \alpha_0)cos(\delta)$, $y = (\delta - \delta_0))$, where (α_0, δ_0) are the Right Ascension and declination of the sources given in Table 1.
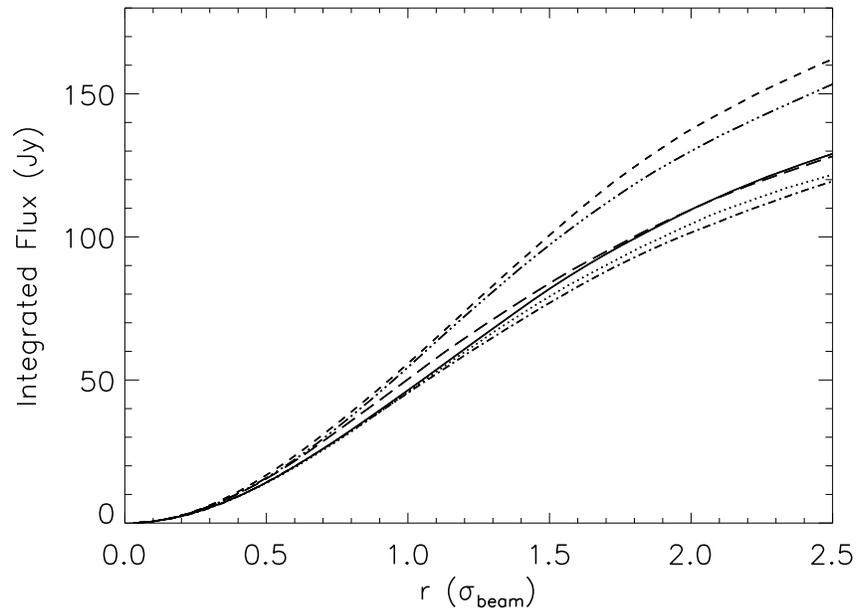
Fig. 2.— Integrated flux vs. radius out from the center of the source for one of the 150 GHz scans of RCW38. The six different curves are for the six 150 GHz channels. Radius is given in units of the beamsize σ_{beam} because the beamsize is slightly different for each channel.
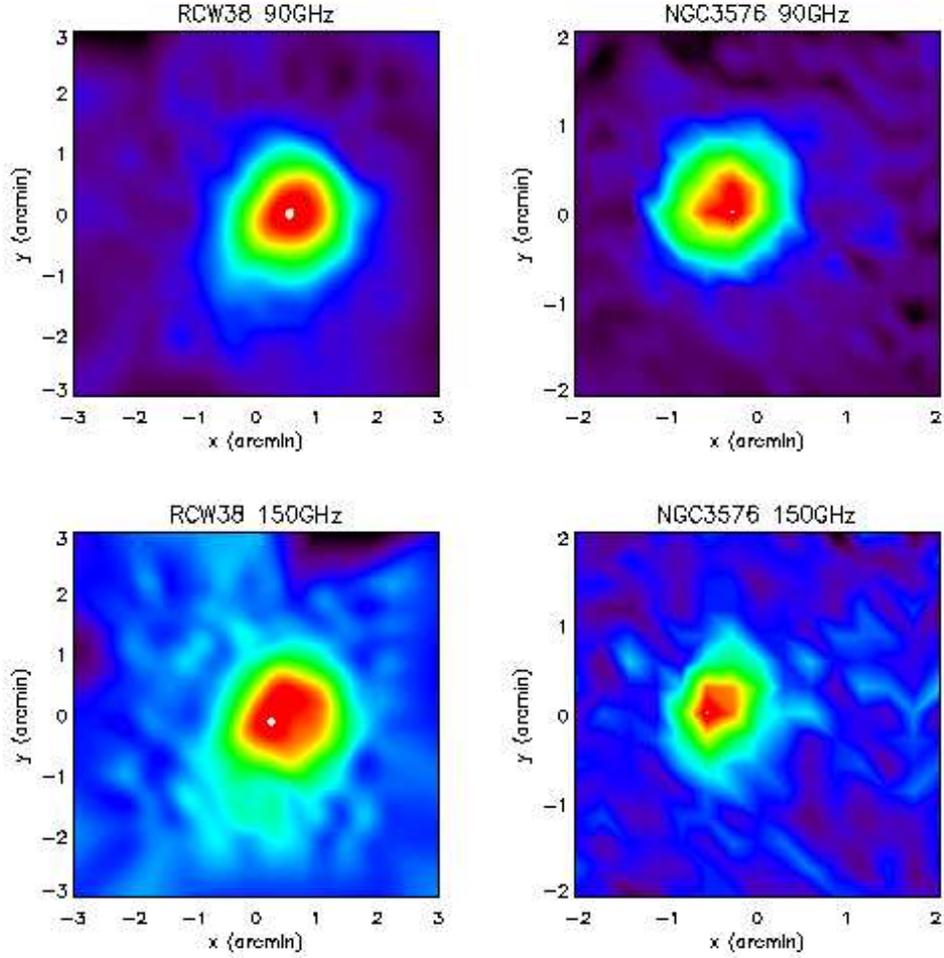
Fig. 3.— SEST maps of compact Galactic sources RCW38 and NGC3576. The maps are flat space projections centered on the source, with coordinates given by ($x = (\alpha - \alpha_0)cos(\delta)$, $y = (\delta - \delta_0)$), where (α_0, δ_0) are the Right Ascension and declination of the sources given in Table 1.
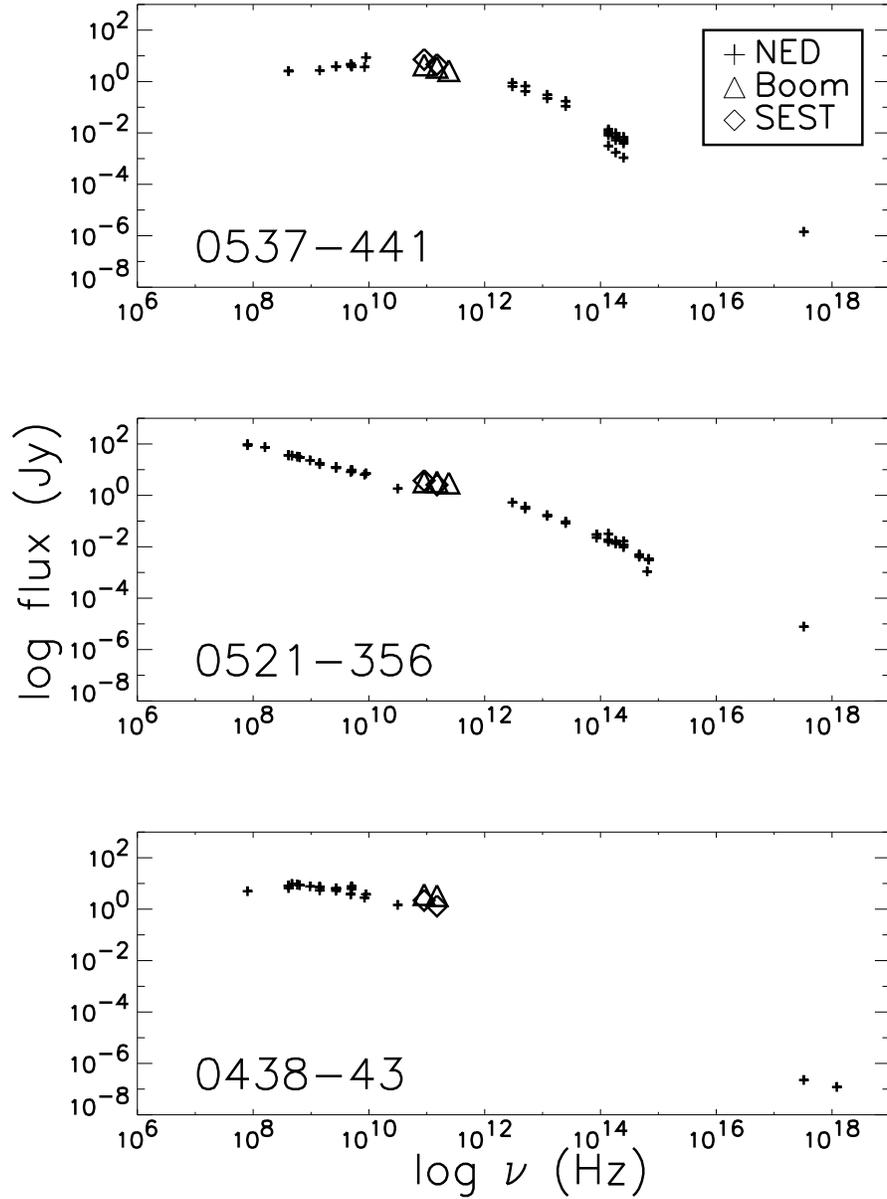
Fig. 4.— Fluxes of extra-galactic sources. BOOMERANG and SEST fluxes for each source are plotted along with measurements over a wide range of the electromagnetic spectrum from the NASA/IPAC Extra-galactic Database (NED).

| Source	RA	Dec	Object Type	N_{90}	N_{150}	N_{240}	N_{400}
Carina	161.06	-59.58	HII Region	2	6	3	4
RCW38	134.77	-47.51	HII Region	8	24	12	16
IRAS1022	156.05	-57.80	HII Region	7	22	11	13
NGC3603	168.79	-61.29	HII Region	2	6	3	4
NGC3576	167.98	-61.33	HII Region	2	6	3	4
IRAS08576	134.86	-43.76	HII Region	10	29	15	19
0537-441	84.71	-44.09	Blazar	2	6	1	0
0521-365	80.74	-36.46	BL Lac	2	5	2	0
0438-43	70.07	-43.55	QSO	1	4	0	0

Table 1: Observed sources. Listed are J2000 coordinates, object type and number of observations by BOOMERANG at each frequency. The total number of observations at each frequency (e.g. N_{90} at 90 GHz) is the number of good scans over all channels at that frequency. Coordinates of Galactic sources are from IRAS maps. Coordinates of extra-galactic sources are from SEST.

Source	90 GHz $1\sigma_b$ (Jy)	90 GHz $2\sigma_b$ (Jy)	150 GHz $1\sigma_b$ (Jy)	150 GHz $2\sigma_b$ (Jy)	240 GHz $1\sigma_b$ (Jy)	240 GHz $2\sigma_b$ (Jy)	400 GHz $1\sigma_b$ (Jy)	400 GHz $2\sigma_b$ (Jy)
Carina	72.4±8.2	214±19	37.9±4.1	131±13	132±18	410±56	446±145	1324±419
RCW38	60.8±6.2	137±16	51.7±4.0	122±12	126±17	298±42	406±115	1002±298
IRAS1022	60.7±4.6	143±15	42.2±2.9	119±11	107±15	282±38	320±94	904±278
NGC3603	55.6±6.1	126±14	42±1.2	107±4.4	101±14	249±35	308±99	802±256
NGC3576	32.6±3.6	74.6±9.1	32.7±1.5	70.1±6.0	87.9±10	201±24	360±102	727±196
IRAS08576	9.1±0.7	20.6±2.6	11.8±0.7	31.9±2.2	55.2±6.3	158±18	230±59	667±173
0537-441	1.8±0.4	3.8±1.1	1.5±0.2	3.1±0.6	1.3±0.8	2.3±2.1	–	–
0521-365	1.5±0.5	2.9±1.4	1.3±0.3	2.9±0.7	1.3±0.7	2.6±0.4	–	–
0438-43	1.4±0.5	3.2±1.3	1.2±0.2	2.9±0.6	–	–	–	–

Table 2: Fluxes in Jy of sources as determined by observations with BOOMERANG. The $1\sigma_b$ and $2\sigma_b$ fluxes are the integrated fluxes within radii of 1 and 2 σ_{beam} respectively. Errors are statistical only; they do not include systematic errors due to uncertainty in the beam size, background subtraction or calibration. For a point source observed with a gaussian beam, the integrated fluxes out to $1\sigma_b$ and $2\sigma_b$ are 0.393 and 0.865 of the source flux, respectively. The extra-galactic sources are point sources, whereas the Galactic sources are somewhat extended.

Source	$\alpha_{90:150}$ $1\sigma_b$	$\alpha_{90:150}$ $2\sigma_b$	$\alpha_{150:240}$ $1\sigma_b$	$\alpha_{150:240}$ $2\sigma_b$	$\alpha_{240:400}$ $1\sigma_b$	$\alpha_{240:400}$ $2\sigma_b$
Carina	-1.3±0.3	-1.0±0.3	3.3±0.5	3.0±0.5	2.0±0.6	2.0±0.6
RCW38	-0.3±0.3	-0.2±0.3	2.3±0.5	2.3±0.5	2.0±0.6	2.0±0.6
IRAS1022	-0.7±0.2	-0.4±0.3	2.4±0.4	2.3±0.5	1.8±0.6	1.9±0.6
NGC3603	-0.6±0.3	-0.3±0.3	2.3±0.4	2.2±0.4	1.9±0.6	2.0±0.6
NGC3576	0.0±0.3	-0.1±0.3	2.6±0.4	2.7±0.4	2.4±0.5	2.2±0.5
IRAS08576	0.5±0.2	0.9±0.3	4.0±0.4	4.2±0.4	2.4±0.5	2.4±0.5
0537-441	-0.4±0.5	-0.5±0.7	-0.4±1.6	-0.7±2.5	–	–
0521-365	-0.3±0.8	0.0±1.0	0.1±1.5	-0.1±2.0	–	–
0438-43	-0.4±0.8	-0.2±0.9	–	–	–	–

Table 3: Spectral indices of sources observed with BOOMERANG. The spectral index $\alpha_{f1:f2}$ between two frequencies $f1$ and $f2$ is computed using eq. 1 and the fluxes in Table 2.

– 17 –

Source	90 GHz (Jy)	150 GHz (Jy)	240 GHz (Jy)	$\alpha_{90:150}$	$\alpha_{150:240}$
0537-441	3.8 ± 0.8	3.6 ± 0.6	2.2 ± 0.4	-0.1 ± 0.5	-0.9 ± 0.6
0521-365	3.4 ± 0.8	2.8 ± 0.4	2.7 ± 0.5	-0.3 ± 0.5	-0.1 ± 0.6
0438-43	2.1 ± 0.5	1.5 ± 0.3	1.0 ± 0.2	-0.6 ± 0.5	-0.8 ± 0.7

Table 4: Total fluxes in Jy and spectral indices of extra-galactic sources observed by BOOMERANG computed using a wavelet analysis.

Source	90 GHz (Jy)	150 GHz (Jy)	$\alpha_{90:150}$
RCW38	125±10	116±7	-0.15±0.20
NGC3576	75±7	78±8	0.08±0.27
0537-441	7.21±0.31	4.59±0.35	-0.9±0.2
0521-365	3.76±0.30	2.55±0.41	-0.8±0.4
0438-43	2.21±0.31	1.33±0.41	-1.0±0.7

Table 5: Fluxes in Jy and spectral indices of sources observed with SEST. Fluxes for RCW38 and NGC3576 are computed for the regions shown in Figure 3. Fluxes for the extra-galactic sources are from point source observations.

Source	B/S 90 GHz $1\sigma_b$	B/S 90 GHz $2\sigma_b$	B/S 150 GHz $1\sigma_b$	B/S 150 GHz $2\sigma_b$
RCW38	1.25±0.17	1.27±0.19	1.15±0.12	1.22±0.15
NGC3576	1.11±0.16	1.15±0.17	1.09±0.12	1.05±0.15
0537-441	0.65±0.14	0.62±0.18	0.85±0.13	0.77±0.15
0521-365	1.02±0.34	0.87±0.42	1.27±0.30	1.33±0.37
0438-43	1.61±0.60	1.69±0.73	2.20±0.79	1.95±0.72

Table 6: Flux ratios of BOOMERANG to the convolution of the SEST data with the BOOMERANG beam: BOOM/(SEST*BOOM). Errors are statistical only; they do not include the systematic error in the fluxes due to uncertainty in the BOOMERANG beam size. The BOOMERANG fluxes used are those from Table 2. The extra-galactic sources may be time variable, and since the BOOMERANG and SEST observations were made approximately a year apart, they could have different intensities not only because of calibration but because of intensity variations.